Research Article

Alexander E. Dudorov* and Sergey A. Khaibrakhmanov

Hierarchical structure of the interstellar molecular clouds and star formation

https://doi.org/10.1515/astro-2017-0428
Received Sep 25, 2017; accepted Nov 16, 2017

Abstract: Properties of the hierarchical structures of interstellar molecular clouds are discussed. Particular attention is paid to the statistical correlations between velocity dispersion and size, and between the magnetic field strength and gas density. We investigate the formation of some hierarchical structures with the help of numerical MHD simulations using the ENLIL code. The simulations show that the interstellar molecular filaments with parallel magnetic field and molecular cores can form via the collapse and fragmentation of cylindrical molecular clouds. The parallel magnetic field halts the radial collapse of the cylindrical cloud maintaining its nearly constant radius $\sim$0.1 pc. The observed filaments with perpendicular magnetic field can form as a result of the magnetostatic contraction of oblate molecular clouds under the action of Alfvén and MHD turbulence. The theoretical density profiles are fitted with the Plummer-like function and agree with observed profiles of the filaments in Gould's Belt. The characteristics of molecular cloud cores found in our simulations are in agreement with observations.

Keywords: Instabilities, Magnetic fields, Magnetohydrodynamics (MHD), Stars: formation, Galaxies: ISM

1 Introduction

Observations of star-forming regions in the Galaxy revealed the hierarchical structure of the interstellar medium (ISM) (Scalo 1985). The superclouds containing complexes of the molecular clouds (also known as Giant Molecular Clouds, like the Gould Belt) are at the top of the hierarchy. Recent high-resolution observations of the Gould Belt found that the parsec-scale filamentary structure is a common feature of the Giant molecular clouds (see review André *et al.* 2014). The filaments are determined as elongated structures in the maps of the interstellar medium. Analysis of the observations has shown that the filaments may have a nearly constant radius $\sim$ 0.1 pc. Polarimetry surveys of the Gould belt indicated that the large-scale magnetic field direction can be both perpendicular and parallel to the axis of a filament (Ward-Thompson *et al.* 2017). These findings rise a question how the different filaments form. Further evolution of the filaments is also of a great interest, as it is now considered that the prestellar and protostellar clouds are the result of the gravitational fragmentation of the filaments. Most of the prestellar and protostellar clouds (the lower level of the ISM's hierarchy) found by Herschel are located inside the filaments (Konyves *et al.* 2015).

We propose that the observed filaments can be either cylinders or flat sheets/disks seen by an observer from the edge. The filamentary structures with the perpendicular magnetic field (like in the Taurus molecular cloud (Chapman *et al.* 2011)) are more likely to be a edge-on disks or sheets, since these configurations are a natural result of the gas contraction along the magnetic field lines. In turn, the cylinders with parallel magnetic field can be unstable with respect to the formation of the gravitational constrictions (Chandrasekhar and Fermi 1953). This process can lead to the formation of prestellar and protostellar cores.

In order to check our hypotheses, we performed two-dimensional numerical magnetohydrodynamical (MHD) simulations of two simplest configurations, namely the high-mass cylinders and flat disks.

Structure of the paper is following. In section 2 we analyse the hierarchical structure of the interstellar magnetic clouds (IMC) and discuss scale correlations for IMC. In section 3 the numerical code used for the simulations is described. Section 4.1 present the results of the numerical simulations of cylindrical molecular cloud collapse. We considered free isothermal collapse (section 4.2) and

Corresponding Author: Alexander E. Dudorov: Chelyabinsk State University, 129 Bratiev Kashirinykh Str., Chelyabinsk 454001, Russian Federation; Email: dudorov@csu.ru

Sergey A. Khaibrakhmanov: Ural federal university Should be: Sergey A. Khaibrakhmanov: 1. Ural Federal University, 19 Mira Str., Ekaterinburg 620000, Russia; 2. Chelyabinsk State University, 129 Bratiev Kashirinykh Str., Chelyabinsk 454001, Russian Federation; Email: khaibrakhmanov@csu.ru

Table 1. The hierarchy of the interstellar magnetic clouds

Hierarchy	Supercloud	Complex of molecular clouds	Molecular cloud	Filament	Prestellar core	Protostellar cloud	Sequence of clouds
T, K	100	15-40	15-40	10-25	10-15	30-100	Warm
		10	8-40			10	Cold
n, cm^{-3}	1	100-300	$10^2 - 10^3$	$10^4 - 10^5$	$10^4 - 10^6$	$10^3 - 10^5$	Warm
		$10^2 - 10^3$	$10^3 - 10^4$			$10^4 - 10^6$	Cold
M, $M_\odot$	$10^7 - 3 \times 10^7$	$8 \times 10^4 - 2 \times 10^6$	$10^3 - 10^5$	200-3000	0.1-10	10-1000	Warm
		$10^3 - 2 \times 10^4$	20-500			0.3-20	Cold
R, pc	$(0.5 - 2) \times 10^3$	30-80	3-30	0.1-10	0.007-0.1	0.5-3	Warm
		3-20	0.2-4			0.05-0.5	Cold
σ_v, km/s	10-20	6-15	4-12	0.2-5	< 0.6	1.5-3	

the collapse of magnetic cylinder (section 4.3). The evolution of the cylindrical cloud with initially perturbed surface is studied in section 4.4. The collapse of the massive disk with initially perpendicular magnetic field is investigated in section 5. We summarize our results in section 6.

2 Hierarchical structure of interstellar magnetic clouds

One of the main properties of the ISM is its hierarchical structure (Scalo 1985). Dudorov (Dudorov 1991) compiled and analysed the observational data on hierarchical structure in the ISM. In the present work, we supplemented the original table of Dudorov (see Table 1 in (Dudorov 1991)) with the characteristics of the filaments and prestellar cores collected from (Yamaguchi *et al.* 1999; André 2006; Roccatagliata *et al.* 2015; Konyves *et al.* 2015; André *et al.* 2016; Cox *et al.* 2016; Kainulainen *et al.* 2016). In Table 1, the first row contains the names of the hierarchy levels (in the descending order with respect to the size of the corresponding structure). The temperatures, densities, masses, sizes and velocity dispersions for each level are listed in rows 2-6, respectively. Rows labelled with "Warm" and "Cold" (the last column) correspond to warm and cold ISM components, respectively. Warm and cold sequences of clouds correspond to the regions of massive star formation (like Orion) and low-mass star formation (like ρ Oph), respectively.

Superclouds are the limiting structure of the hierarchy. The superclouds are two-dimensional flat structures with diameters $\sim$ 1 kpc and heights < 100 pc formed as a result of the gravitational instability in the magnetic galaxy discs with spiral arms (Elmegreen 1989). The famous example of a supercloud is the Gould Belt. The flatter mode of the superclouds leads to the formations of the cylindrical complexes of the molecular clouds (Dudorov 1991). The complexes fragment into the three-dimensional molecular clouds. The densest regions of the MC can collapse into the protostellar clouds.

Recent high-resolution studies of the nearest star-forming clouds of the Galaxy at submillimetre wavelengths with the Herschel Space Observatory have demonstrated that the filamentary structure is the common feature of the GMCs in our Galaxy (see review (André *et al.* 2014)). Table 1 shows that the filaments can be identified as the densest molecular clouds in the complexes. The filaments can possibly form similarly to the the cylindrical complexes of the molecular clouds.

The prestellar cores can be described as the molecular cloud cores, that are stationary and not massive enough to undergo the gravitational collapse.

Scale correlations are important for the interpretation the formation of the hierarchy. The correlation between size R and velocity dispersion σ_v is the most reliable one. It can be defined as (Scalo 1987)

$$\sigma_v = R^{q_\sigma}, \tag{1}$$

where $q_\sigma = 0.3 - 0.7$. The $\sigma_v(R)$ correlation is used to assess the properties of the turbulence in the interstellar clouds (Larson 1981). Kolmogorov's turbulence is characterized by $q_\sigma = 1/3$, $q_\sigma = 0.25$ characterizes the MHD wave (Kreichnan's) turbulence, $q_\sigma = 1$ corresponds to the two-dimensional turbulence, 0.7 – intermittent turbulence.

Dudorov (Dudorov 1991) has shown that the variations of the q_σ through the hierarchy can be explained by the change in the magnetic field role along the hierarchy. The dependence of the magnetic field strength on density can be written as

$$\frac{B}{B_0} = \left(\frac{n}{n_0}\right)^{k_B}, \tag{2}$$

where B_0 and n_0 characterize the initial conditions of the cloud formation. Parameter k_B depends on the symmetry of the flow and lies in range $[0, 1]$. Contraction along the

Table 2. The parameters of scale correlations of the interstellar magnetic clouds

Hierarchy	Supercloud	Complex of molecular clouds	Molecular cloud	Protostellar cloud	Sequence of clouds
q_σ	1	0.7-1	0.4-0.6	0.2-0.4	Warm
		0.6-0.7	0.3-0.4	0.2-0.3	Cold
k_B	0	1/3-2/3	1/2-2/3	2/5-2/3	

magnetic field lines is characterized by $k_B = 0$. The motion perpendicular to the magnetic field lines corresponds to $k_B = 1$. Spherically symmetric flow has $k_B = 2/3$. Averaging over all angles between the magnetic field and velocity gives $k_B = 1/3$.

Dudorov (Dudorov 1990) collected observational data on the magnetic field in the interstellar clouds and revealed three main sequences

$$(B_0,\ n_0,\ k_B) = (3 - 5\,\mu\mathrm{G},\ -,\ 0), \tag{3}$$

$$(B_0,\ n_0,\ k_B) = (3 - 5\,\mu\mathrm{G},\ 10 - 20\,\mathrm{cm}^{-3},\ 1/2), \tag{4}$$

$$(B_0,\ n_0,\ k_B) = (3 - 5\,\mu\mathrm{G},\ 10 - 20\,\mathrm{cm}^{-3},\ 2/3). \tag{5}$$

The first sequence explains the formation of the flat layers due to one-dimensional flows along the magnetic field lines. The clouds with $k_B = 1/2$ can form as a result of the quasi-static contraction under the control of the magnetic field. In the dense clouds, magnetic ambipolar diffusion slows down the growth of the magnetic field strength ($k_B = 2/5$). Then the role of the magnetic field weakens, plasma beta becomes $\beta > 1$, and the evolution of the cloud takes place along the third sequence with $k_B = 2/3$. Thus, the magnetic field strength changes along the hierarchy.

Values of the correlation parameters q_σ and k_B for different levels of the hierarchy are listed in Table 2. All kinds of turbulence exist in the ISM, according to this table. Not only the burst processes, jets, outflows, but also the MHD instabilities and waves can be the source of the turbulence.

The correlation parameter q_σ changes along the hierarchy in accordance with the changing role of the magnetic field. The superclouds and some complexes of the molecular clouds are characterized by $\beta \ll 1$ and $k_B \simeq 0$. The induced turbulence in this case is more likely to be two-dimensional ($\sigma_v = 1$). Kolmogorov's turbulence ($\sigma_v = 1/3$) is found on the scales of molecular clouds and their cores. The turbulence in the magnetostatic molecular clouds is characterized by $\sigma_v = 0.5$. The increase of σ_v at large scales of the hierarchy can be explained by the effects of compressibility and intermittency of the turbulence.

3 Numerical model

In this section, we present the numerical model used to investigate the evolution of the molecular clouds in the form of a cylinders and flat disks. We investigate the effect of the magnetic field on the cloud collapse and study the growth of small perturbations during the collapse.

3.1 Governing equations

We investigate the evolution of the molecular clouds using the system of ideal MHD equations

$$\frac{\partial \rho}{\partial t} + \mathrm{div}\,(\rho \mathbf{v}) = 0, \tag{6}$$

$$\rho \frac{\partial \mathbf{v}}{\partial t} + (\rho \mathbf{v} \nabla)\,\mathbf{v} = -\nabla P - \rho \nabla \Phi + \frac{1}{4\pi}\,[\mathrm{rot}\,\mathbf{B}, \mathbf{B}]\,, \tag{7}$$

$$\rho \left[\frac{\partial \varepsilon}{\partial t} + (\mathbf{v} \cdot \nabla)\,\varepsilon\right] + P \nabla \cdot \mathbf{v} = 0, \tag{8}$$

$$\frac{\partial \mathbf{B}}{\partial t} = \mathrm{rot}\,[\mathbf{v}, \mathbf{B}]\,, \tag{9}$$

$$\nabla^2 \Phi = 4\pi G \rho, \tag{10}$$

$$P = (\gamma - 1)\varepsilon\rho, \tag{11}$$

where Φ is the gravitational potential, ε the gas internal energy, γ the adiabatic index. All the remaining quantities are used in their usual notation.

3.2 Numerical code

The numerical solution of the model equations is realized in the code ENLIL. This is a two-dimensional code for modelling the axysymmetric MHD flows (Dudorov *et al.* 1999; Zhilkin *et al.* 2009). The code is based on the explicit quasi-monotonic TVD-scheme of high order of accuracy. The HLLD-solver is used for solving the hyperbolic subsystem of the equations. Divergence cleaning is performed via the method of generalized Lagrangian multipliers. Poisson's equation is solved using the alternating directions method.

4 Collapse of a cylinder

4.1 Parameters

We consider the collapse of non-rotating cylinder with initial length $H_0 = 5$ pc, cross-section radius $R_0 = 0.2$ pc, density $n_0 = 10^5$ cm^{-3}, temperature $T_0 = 10$ K. The mass of the cloud is $7.7 \times 10^3\ M_\odot$. The corresponding relation of the thermal energy to the modulus of the gravitational energy is $\varepsilon_{th} = 3 \times 10^{-3}$.

Cylindrical coordinates $\{r, \varphi, z\}$ are used. We consider axisymmetric motions in $r - z$ plane. The axis of the cylinder is directed along the z-axis. The simulation box is a square with size 5.2 pc. The resolution $(N_r, N_z) = (400, 100)$ was used in all calculations of the cylindrical cloud collapse, where N_r and N_z are the cells number in r-direction and z-direction. We adopted a Courant number of 0.1.

4.2 Free isothermal collapse

First, let us consider the collapse of the isothermal cylinder without the magnetic field. In equation 11, adiabatic index is adopted to be equal to 1.001 which corresponds to nearly isothermal gas. In Figure 1, we plot the evolution of the radial profiles of the gas concentration in the $z = 0$ plane. The initial profile is black.

Figure 1 shows that the cylinder's radius decreases and density grows during the collapse. By the end of the simulation, $t = 9.9 \times 10^4$ yrs (orange line in figure 1), the density grows by five orders of magnitude at the cloud's axis.

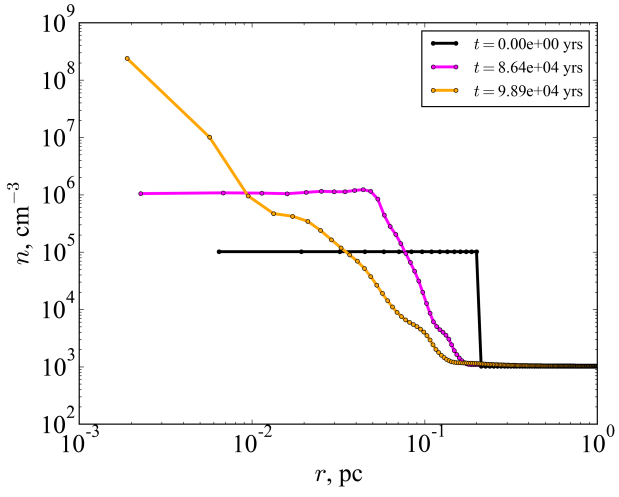

Figure 1. The $n(r, z = 0)$ dependences for the isothermal cylinder without magnetic field at $t = 0$ (black), $t = 8.64 \times 10^4$ yrs (magenta) and $t = 9.89 \times 10^4$ yrs (orange) after the beginning of the collapse.

In the collapsing cylinder, the ratio of pressure gradient force, $F_P = \nabla P/\rho$, to gravitational force, $F_g = \nabla\Phi$, changes with the cloud's radius R as

$$\frac{F_P}{F_g} \propto R^{2-2y}. \tag{12}$$

Therefore, the gravitational collapse of a cylinder will be stopped for any $y > 1$.

4.3 Magnetic cylinder

Consider the evolution of the cylindrical molecular cloud with the magnetic field directed along the cloud's axis, $\mathbf{B_0} = (0, 0, B_0)$. The initial magnetic field is 1.9×10^{-4} G, such that the ratio of magnetic energy to the modulus of gravitational energy $\varepsilon_m = 0.03$. The adiabatic index is 5/3.

In Figure 2, we plot two-dimensional distributions of cloud's gas number density and magnetic field at $t = 0$ yrs, $t = 1.21 \times 10^5$ yrs and 3.72×10^5 yrs. The left panel represents the initial state of the cloud. At the initial stages, $t < 10^5$ yrs, the cloud radially collapses and its density increases everywhere. The magnetic pressure in the radially collapsing cylinder grows approximately as

$$P_m \propto \rho^2, \tag{13}$$

so the effective adiabatic index of the cylinder with magnetic field is nearly 2. According to (12), the magnetic pressure gradient halts the gravitational collapse even in the isothermal case around $t \simeq 10^5$ yrs. After that, the cloud begins to pulsate, so that its radius and density periodically change. Slow contraction of the cloud proceeds along the z-axis, as the electromagnetic force does not influence the gas motion in this direction. At the end of the simulation, $t = 3.7 \times 10^5$ yrs, the height of the cylinder decreased by ~20%.

Figure 3 depicts the radial density profiles in the $z = 0$ plane. Figure 3 shows that density grows 10 times compared to the initial value by $t = 1.2 \times 10^5$ yrs. After that, the cloud expands and its density decreases.

The radial profiles of the filaments are usually fitted by a Plummer-like function of the form (see (André *et al.* 2014))

$$n(r) = n_c \left(1 + \left(\frac{r}{r_0}\right)^2\right)^{-p/2}. \tag{14}$$

where n_c is the central density of the filament, r_0 the radius of the flat inner region, p the power-law exponent at $r \gg r_0$. Profiles depicted in figure 3 can be fit with $p = 2$ and $r_0 = 0.1$ pc, in the agreement with the typical values obtained from the observations (André *et al.* 2014).

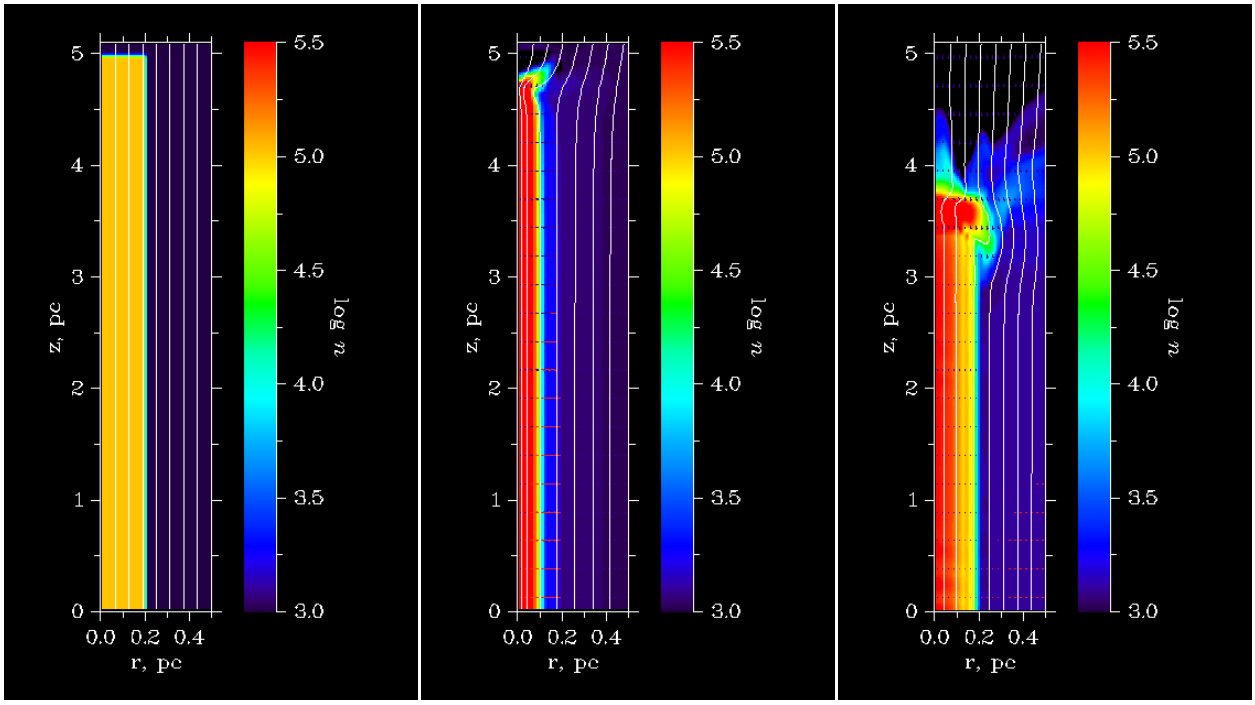

Figure 2. Two-dimensional concentration (color filling) and magnetic field (white isolines) distributions for the adiabatic cylinder with magnetic field at $t = 0$ yrs (initial state, left), $t = 1.21 \times 10^5$ yrs (center), 3.72×10^5 yrs (right) after the beginning of the collapse.

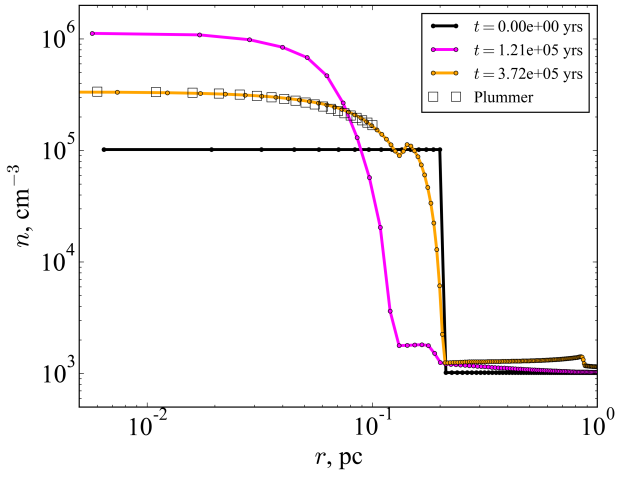

Figure 3. The $n(r, z = 0)$ dependences for the adiabatic cylinder with magnetic field at $t = 0$ (black), $t = 1.21 \times 10^5$ yrs (magenta) and $t = 7.72 \times 10^5$ yrs (orange) after the beginning of the collapse. Blanck squares depict a Plummer-like function (14) with $p = 2$, $r_0 = 0.1$ pc.

4.4 Role of perturbations

In this section, we study the formation of the gravitational "sausages" of Chandrasekhar and Fermi (Chandrasekhar and Fermi 1953) and subsequent fragmentation of the cylindrical clouds and formation of the molecular cloud cores.

We introduce the perturbation of the initial cylinder's boundary, following Chandrasekhar and Fermi (Chandrasekhar and Fermi 1953). The radius of the perturbed cylinder R is determined from the relations

$$r = R + a\cos(kz), \tag{15}$$

$$R_0^2 = R^2 + a^2/2, \tag{16}$$

where a is the perturbation amplitude, k the wave number. The initial magnetic field has the components $\mathbf{B} = (b_r, 0, B_0 + b_z)$ in this case, where the small fluctuating components are

$$b_r = aA_1 I_1(kr)\sin(kz) + a^2 A_2 I_1(2kr)\sin(2kz), \tag{17}$$

$$b_z = aA_1 I_0(kr)\cos(kz) + a^2 A_2 I_0(2kr)\cos(2kz), \tag{18}$$

with

$$A_1 = -\frac{B}{R}\frac{kR}{I_1(kR)}, \tag{19}$$

$$A_2 = \frac{B}{R^2}\frac{kR}{I_1(2kR)}\left(\frac{kRI_0(kR)}{I_1(kR)} - \frac{1}{2}\right), \tag{20}$$

$$B = B_0\left(1 + \frac{a^2}{R^2}\frac{kRI_0(kR)}{I_1(kR)}\right), \tag{21}$$

and I_0, I_1 are the Bessel functions of the first kind.

For the simulation, we have chosen the same cloud's parameters, as in section 4.3. The initial amplitude of the perturbations is set to $a = 0.1R_0$. The wavelength of the

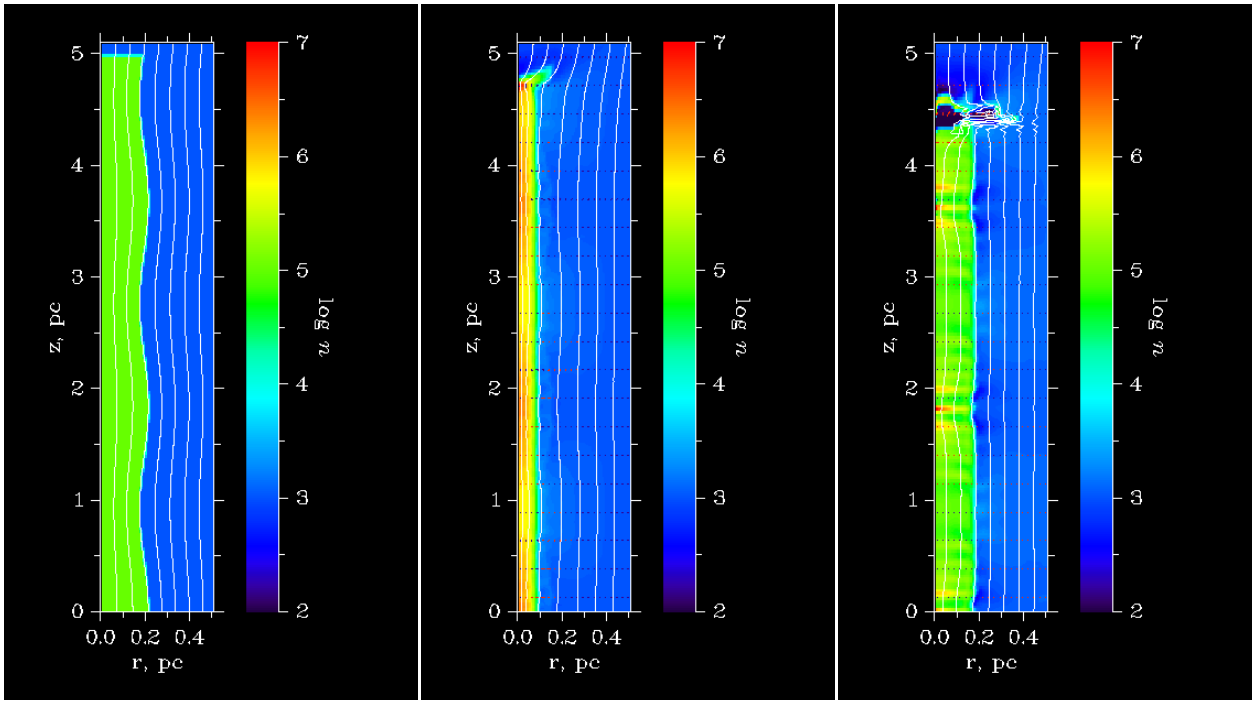

Figure 4. Two-dimensional density (color filling) and magnetic field (white isolines) distributions for the initially perturbed adiabatic cylinder with magnetic field at $t = 0$ yrs (initial state, left), $t = 1.17 \times 10^5$ yrs (center), 1.77×10^5 yrs (right) after the beginning of the collapse.

perturbation is adopted to be $k = 0.47/R$, which corresponds to the fastest growing mode at $B_0 = 1.9 \times 10^{-4}$ G.

In figure 4, we plot two-dimensional distributions of cloud's density and magnetic field at $t = 0$ yrs, $t = 1.17 \times 10^5$ yrs and 1.77×10^5 yrs. The initial evolution of the cloud is similar to the evolution of the unperturbed cylinder (section 4.3). The cloud collapses and the magnetic pressure gradient stops the collapse after $t \simeq 10^5$ yrs.

Growth of the initial perturbations leads to the formation of the gravitational "sausages" and subsequent gravitational fragmentation of the cloud, which is clearly seen in the right panel of figure 4 ($t = 1.77 \times 10^5$ yrs). The characteristics of the fragments are listed in table 3. Table shows that temperatures, densities, masses and radii of the fragments are in agreement with the corresponding characteristics of the protostellar clouds.

Table 3. Characteristics of the fragments found in simulations (column 3) in comparison with the protostellar clouds' properties (column 2)

	Protostellar cloud	Clumps
T, K	30-100 10	20-500
n, cm^{-3}	$10^3 - 10^5$ $10^4 - 10^6$	$5 \times 10^7 - 5 \times 10^8$
M, $M_\odot$	10-1000 0.3-20	$\sim 100 - 1000$
R, pc	0.5-3 0.05-0.5	0.05 – 0.1

5 Collapse of disk

In this section, we consider the evolution of a disk with a perpendicular magnetic field. The disk equatorial plane coincides with $z = 0$ plane. The disk has radius $R_0 = 5$ pc and height $H_0 = 0.2$ pc. The mass of the disk with initial $T_0 = 10$ K and $n_0 = 10^5$ cm^{-3} is $1.9 \times 10^5 M_\odot$. The initial ratio of thermal energy to the modulus of the gravitational energy is $\varepsilon_{th} = 2.7 \times 10^{-4}$, and initial ratio of the magnetic energy to the modulus of the gravitational energy $\varepsilon_m = 0.1$ ($B_0 = 1.1 \times 10^{-3}$ G). The adiabatic index is $\gamma = 5/3$. The computational domains has size 5.1 pc and the resolution $(N_r, N_z) = (100, 400)$.

In figure 5, we plot two-dimensional distributions of cloud's density and magnetic field at $t = 0$ yrs, $t = 9.61 \times 10^4$ yrs and 1.48×10^5 yrs. At the initial stages of the evolution, $t < 10^5$ yrs, the disk contracts along the z-axis. After that, the adiabatic pressure gradient halts the contraction and the collapse turns to expansion and subsequent pulsations.

Figure 5 shows that the initial vertical magnetic field acquires the quasi-radial geometry near the disk bound-

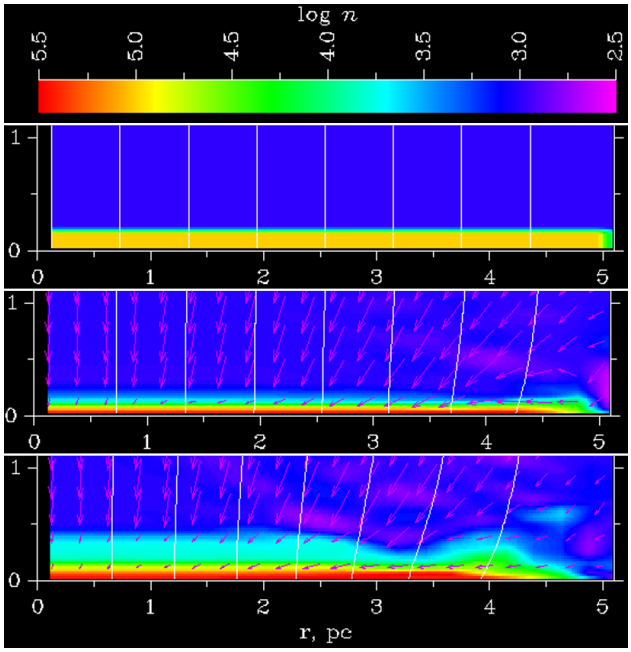

Figure 5. Two-dimensional concentration (color filling) and magnetic field (white isolines) distributions for the adiabatic disk with initially perpendicular magnetic field at $t = 0$ yrs (initial state, top), $t = 9.61 \times 10^4$ yrs (middle), 1.48×10^5 yrs (bottom) after the beginning of the collapse.

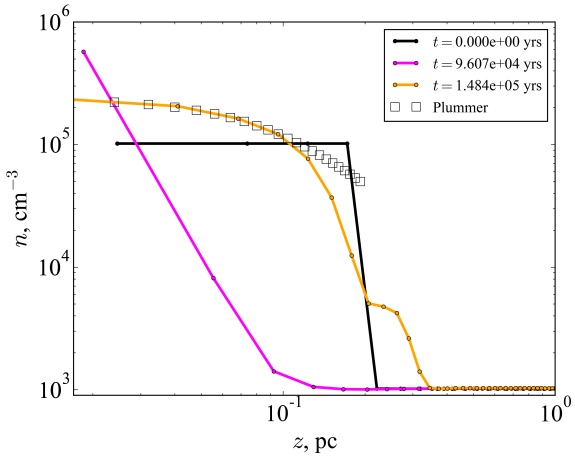

Figure 6. The $n(r = 0, z)$ dependences for the adiabatic disk with initially perpendicular magnetic field at $t = 0$ (black), $t = 9.61 \times 10^5$ yrs (magenta) and $t = 1.48 \times 10^5$ yrs (orange) after the beginning of the collpase. Blanck squares depict a Plummer-like function with power-law exponent $p = 2$ and height scale 0.1 pc.

ary with time due to a slow radial contraction. The density achieves a maximum at $r \simeq 3-3.5$ pc, as this regions contracts in both radial and vertical directions.

In Figure 6 we depict the vertical profiles of the gas concentration in the $r = 0$ plane at the times as in Figure 5. The figure shows that the disk's central density grows by approximately one order of magnitude during the initial stage of collapse. After that, the collapse stops and the disk relaxes to a Plummer-like density distribution (14) with $p = 2$ and r/r_0 replaced by z/z_0, $z_0 = 0.1$.

6 Conclusions and discussion

We analyse the properties of the interstellar molecular clouds and the hierarchical structure of the ISM. Dudorov (Dudorov 1991) has shown that the magnetic field strength varies through the hierarchy and it plays determining role in the formation of the hierarchical structures. Turbulence properties are also determined by the action of the magnetic field at the different levels of the hierarchy.

We perform numerical simulations of the collapse of cylinders with parallel magnetic field and adiabatic disks with perpendicular magnetic fields. Optically thick parts of the cylindrical cloud represents the filament. The gravitational fragmentation of the filaments and formation of the cores of molecular clouds are investigated.

The magnetic field hinders the radial collapse of the cylindrical cloud and allows the filament to maintain the constant radius $\sim 0.05-0.1$ pc found in observations (André *et al.* 2014). Magnetic pressure grows faster than the gravity in the radially collapsing cylinder, so the magnetic field determines the radius of the filament.

Flat or oblate clouds with perpendicular magnetic fields contract along the magnetic field lines mainly and relaxes to the quasi-stationary disk with nearly constant height ~ 0.1 pc. Observed filaments with perpendicular magnetic field (like in Taurus (Palmeirim *et al.* 2013)) can be considered as the edge-on disks. The constant height of the filament can be also determined by the generation of non-linear MHD waves and turbulence (Vainshtein 1983).

Our calculated density profiles of filaments are fitted by Plummer-like functions with parameters $p = 2$ and $r_0 = 0.1$ pc that are in agreement with observations. However, it should be noted that distribution of mean filaments width may be broader than determined in observations (Panopoulou *et al.* 2017).

We studied the formation of gravitational "sausages" in the cylindrical clouds with initially perturbed surfaces that are in the process of their gravitational collapse. Our simulations show that the gravitational fragmentation of the filaments with parallel magnetic field leads to the formation of molecular clouds cores (as was predicted by Dudorov (Dudorov 1991)). The sizes, masses, temperatures and densities of the cores are in agreement with observations.

In future, we plan to perform more accurate simulations of the cylindrical and disk-like molecular clouds taking into account the diffusion of the magnetic field and radiation transfer.

Acknowledgment: The investigation of the protostellar disks evolution (section 5) is supported by Russian science foundation (project 15-12-10017). The authors thank prof. Andrey M. Sobolev for stimulating conversations.

References

André, Ph. 2006, In: Elmegreen B. G. (Ed.), Proceedings IAU Symposium No. 237 (14-18 August 2006, Praha, Czech Republic), Cambridge University Press, 132-140.

André, P., Di Francesco, J., Ward-Thompson, D., Inutsuka, S.-I., Pudritz, R. E., Pineda, J. E. 2014, From Filamentary Networks to Dense Cores in Molecular Clouds: Toward a New Paradigm for Star Formation, In: Henrik Beuther, Ralf S. Klessen, Cornelis P. Dullemond, and Thomas Henning (Eds.), Protostars and Planets VI (Univ. of Arizona Press, Tucson), 914, 25-51.

André, P., Reveret, V., Könyves, V., Arzoumanian, D., Tige, J., Gallais, O., et al., 2016, A&A, 592, A54.

Chapman, N.L., Goldsmith, P.F., Pineda, J.L., Clemens, D.P., Li, D., Krčo, M. 2011, ApJ, 741, 21.

Chandrasekhar, S. and Fermi, E., 1953, ApJ, 118, 116-141.

Cox, N.L.J., Arzoumanian, D., André, Ph., Rygl, K.L.J., Prusti, T., Men'shchikov, A., et al. 2016, A&A, 590, A110.

Dudorov, A. E. and Sazonov, Y. V. 1987, Nauchnye Inf., 63, 68-86.

Dudorov, A.E. 1990, Itogi Nauki Tekh., Ser. Astron., 39, 77 (in Russian).

Dudorov, A.E. 1991, Sov.Astron., 35, 342-348.

Dudorov, A.E., Zhilkin, A.G., Kuznetsov, O.A. 1999, Matem. Modelir., 11, 101-116 (in Russian).

Elmegreen, B.G. 1989, ApJ, 338, 178-196.

Kainulainen, J., Hacar, A., Alves, J., Beuther, H., Bouy, H., Tafalla, M. 2016, A&A, 586, A27.

Konyves, V., André, Ph., Men'shchikov, A., Palmeirim, P., Arzoumanian, D., Schneider, N., et al. 2015, A&A, 584, A91.

Larson, R.B., 1981, Mon. Not. R. Astr. Soc., 194, 809-826.

Palmeirim, P., André, Ph., Kirk, J., Ward-Thompson, D., et al. 2013, A&A, 550, A38.

Panopoulou, G. V., Psaradaki, I., Skalidis, R., Tassis, K., Andrews, J. J., 2017, MNRAS, 466, 2529-2541.

Roccatagliata, V., Dale, J.E., Ratzka, T., Testi, L., Burkert, A., Koepferl, C., et al. 2015, A&A, 584, A119.

Scalo, J. M. 1985, In: Black D.C. and Mathews M.S. (Eds.), Protostars and Planets II (University of Arizona Press, Tucson), 201-296.

Scalo, J. M. 1987, In: Proceedings of the Interstellar processes Symposium (July 1-7, 1986, Grand Teton National Park, WY), D. Reidel Publishing Co., Dordrecht, 349-392.

Scoville, N. Z., Sanders, D.B. 1987, In: Proceedings of the Interstellar processes Symposium (July 1-7, 1986, Grand Teton National Park, WY), D. Reidel Publishing Co., Dordrecht, 21-50.

Spitzer, L. 1978, Physical Processes in the Interstellar Medium, New York Wiley-Interscience.

Vainshtein, S.I. 1983, Magnetic Fields in Space, Nauka, Moscow (in Russian).

Ward-Thompson, D., Pattle, K., Bastien, P., Furuya, S., et al. 2017, ApJ, 842, 66.

Yamaguchi, N., Mizuno, N., Saito, H., Matsunaga, K., Mizuno, A., Ogawa, H., et al. 1999, PASJ, 51, 775-790.

Zhilkin, A.G., Pavlyuchenkov, Ya.N., Zamozdra, S.N. 2009, Astron. Rep., 53, 590-604.